Chinese Chemical Letters 32 (2021) 53–56

Contents lists available at ScienceDirect

Chinese Chemical Letters

journal homepage: www.elsevier.com/locate/cclet

Communication

Potential active sites of Mo single atoms for electrocatalytic reduction of N_2

Lei Chen[a,1], Chaozheng He[b,d,1], Ran Wang[b,1], Qian Li[a,e], Jian Zeng[a], Wei Liu[c], Yuchao Wang[a,e], Qichen Wang[a], Tong Ye[a], Yougen Tang[a], Yongpeng Lei[a,*]

[a] State Key Laboratory of Powder Metallurgy, Hunan Provincial Key Laboratory of Chemical Power Sources, College of Chemistry and Chemical Engineering, Central South University, Changsha 410083, China
[b] Institute of Environmental and Energy Catalysis, School of Materials Science and Chemical Engineering, Xi'an Technological University, Xi'an 710021, China
[c] State Key Laboratory of Fine Chemicals, Department of Chemistry, School of Chemical Engineering, Dalian University of Technology, Dalian 116024, China
[d] Shaanxi Key Laboratory of Optoelectronic Functional Materials and Devices, School of Materials Science and Chemical Engineering, Xi'an Technological University, Xi'an 710021, China
[e] School of Material Science and Engineering, Central South University of Forestry and Technology, Changsha 410004, China

ARTICLE INFO

Article history:
Received 16 October 2020
Received in revised form 2 November 2020
Accepted 5 November 2020
Available online 5 November 2020

Keywords:
Single atom catalysts
N_2 reduction reaction
Electrocatalysis
Density functional theory
Active sites

ABSTRACT

Single atom catalysts (SACs) with isolated metal atoms dispersed on supports exhibit distinctive performances for electrocatalysis reactions. The designable realization of well-dispersed single metal atoms is still a great challenge owing to their ease of aggregation. Here, Mo single atomic sites (Mo-N_3C) combined with some ultrasmall Mo_2C/MoN clusters (Mo-SA/Mo_2C-MoN-Cs, mean diameter < 2 nm) on nitrogen-doped porous carbon were synthesized *via* a simple pyrolysis of bimetallic Zn/Mo metal-organic frameworks. X-ray absorption near edge spectra (XANES) in combination with various characterizations show that most of Mo species in sample exist in the form of single sites and the exact structure is Mo-N_3C. Density functional theory (DFT) calculation further shows that as the number of N-coordination in the Mo-N_xC moieties increases, the positive charge of Mo atoms increases. The single Mo atoms in Mo-N_3C have the best capability of N_2 adsorption, which may serve as main active sites for further electrochemical N_2 reduction.

It is well established that downsizing the metal nanoclusters to isolated individual atoms is one of the most efficient approach to achieve maximal metal utilization [1–3]. To date, a broad range of single atom catalysts (SACs) with isolated metal atoms on supports have been developed in electrochemical energy conversion and storage [4–7]. Recently, electrochemical N_2 reduction reaction (NRR) to produce ammonia (NH_3) at room temperature and atmospheric pressure has received great attention [8–10]. Tremendous efforts have been focused on exploring a wide range of potential NRR catalysts [11–13], such as precious metals, earth-abundant metal compounds, and metal-free materials. Apparently, electrochemical NRR has great potential as an alternative to traditionally industrial Haber-Bosch process involving in high temperature (> 300 °C), pressure (> 10 MPa) and undesirable by-products [14]. Nonetheless, to date, its low N_2 adsorption, activation capacity and sluggish reaction kinetics need to be resolved urgently [8]. To overcome above drawbacks, great efforts using SACs for NRR have been made. For example, Zhao *et al.* [15] synthesized Fe single atoms supported on lignocellulose-derived carbon with Fe-$(O\text{-}C_2)_4$ as the active sites for NRR. Liu and coworkers [16,17] also reported that Ag single sites (Ag-N_4) and Fe single sites (Fe-N_4) with excellent performance in NRR verified by experiment and theory.

We notice that Mo-based SACs show wide application in electrocatalytic reactions, such as O_2 reduction reaction [18], H_2 evolution reaction (HER), [19,20]. Most recently, Xin *et al.* [21] reported single Mo atoms as a cost-effective catalyst for NRR. Inspired by the above works, the deep understanding of which kind of single Mo sites in Mo-N-C system is good for NRR is urgent. Herein, Mo single atomic sites (Mo-N_3C) combined with some ultrasmall Mo_2C/MoN clusters (mean diameter < 2 nm) were synthesized *via* a simple pyrolysis of bimetallic Zn/Mo metal-organic frameworks. Through density functional theory (DFT) calculation, as the number of N-coordination in the chemical structure of the Mo-N_xC moieties increases, the positive charge of

* Corresponding author.
E-mail address: lypkd@163.com (Y. Lei).
[1] These authors contribute equally to this study.

https://doi.org/10.1016/j.cclet.2020.11.013
1001-8417/

the Mo active sites increases, thereby enhancing the activation degree of N_2 molecules.

The sample (denoted as Mo-SA/Mo_2C-MoN-Cs) synthesized here was firstly characterized to obtain the Brunauer-Emmett-Teller (BET) specific surface area and BJH pore-size distribution (Fig. 1a). According to IUPAC classification, the isotherm of Mo-SA/Mo_2C-MoN-Cs displays a typical type-IV isotherm with a hysteresis loop in the range of $P/P_0 = 0.42 \sim 0.90$. Furthermore, two distinct pores with diameters of 0.9 and 3.8 nm were observed, revealing the coexistence of micropores and mesopores, which was conducive to stability and accessibility of active sites to substrate (Fig. 1b) [22]. Benefiting from the porous nanostructure, the sample displays a BET specific surface area of 845.4 m^2/g. Generally, ZIF-8 derived material has many advantages, such as controllable size and shape, large specific surface area [23–25]. The large surface area is helpful for the active sites to fully contact with electrolyte to improve catalytic activity.

X-ray diffraction (XRD) patterns were then measured to further investigate the structure and composition. In Fig. 1c, only two broad diffraction peaks located at 26° and 43°, corresponding to the graphite structure (002) and (100) planes of carbon frameworks, respectively. No characteristic peaks indexed to metal zinc or zinc oxide are detected, indicating the removal of Zn species from ZIF-8 by the heat treatment at 900 °C. More importantly, there are no obvious characteristic peaks related to Mo_2C and MoN, manifesting the high dispersion and low content of Mo species in carbon matrix. The nature of carbon was further investigated by Raman spectroscopy. In Fig. 1d, the strong peaks located at around 1351 and 1592 cm^{-1} were assigned to disorder carbon and graphitic carbon, respectively. The intensity ratio of the D-band to G-band was calculated to be 1.36, demonstrating highly defective structure [26].

Transmission electron microscopy (TEM) and high angle annular dark field scanning transmission electron microscopy (HAADF-STEM) measurements were performed. As depicted in TEM image (Fig. 2a), the porous carbon with an average size of around 120 nm has a polyhedral morphology and its structural integrity and monodisperisty are well maintained. Furthermore, numerous distinct nanovoids (highlighted by white circles in Fig. 2b) distributed over the entire areas of dispersed polyhedrons, which may be caused by the releasing of gas and evaporation of zinc, accounting for the presence of mesopores [24]. Additionally, in mapping images (Fig. 2c), the Mo, C and N elements uniformly

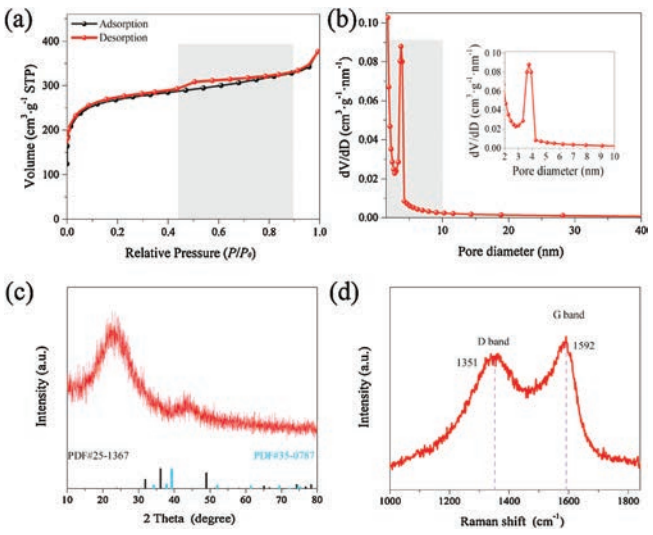

Fig. 1. (a) N_2 adsorption/desorption isotherms, (b) Pore size distribution, (c) XRD patterns, (d) Raman spectra of Mo-SA/Mo_2C-MoN-Cs.

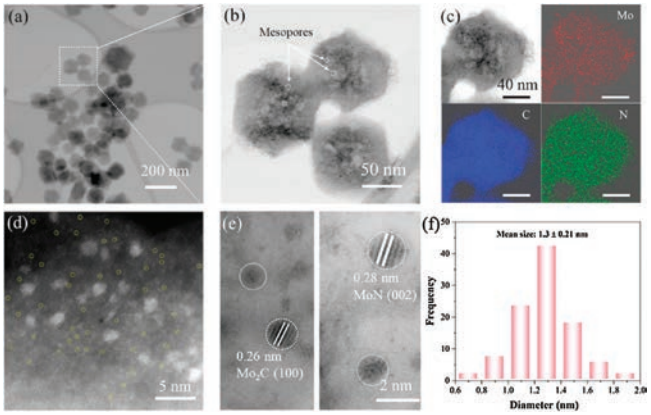

Fig. 2. (a, b) TEM images, (c) HAADF-STEM image and corresponding elemental mapping of Mo-SA/Mo_2C-MoN-Cs. HAADF-STEM images for (d) single Mo atoms and (e) Mo_2C and MoN clusters (yellow circles indicate the distribution of the Mo single atoms and the white circles represent the presence of the atomically dispersed Mo_2C or MoN clusters). (f) Size distribution of Mo_2C or MoN clusters.

distributed through the whole dodecahedrons. Notably, Figs. 2d and e show the representative HAADF-STEM images. The isolated Mo single atoms together with clusters are clearly identified. Specifically, Mo species at an atomic level are uniform monodispersed (the isolated white dots assigned to Mo atoms are labeled in yellow circles for better observation). Meanwhile, white circled parts reveal sharp lattice spacing values of 0.26 and 0.28 nm, associated with (100) and (002) facets of hexagonal Mo_2C (PDF#35-0787) and MoN (PDF#25-1367), respectively. The diameter of Mo_2C and MoN clusters are found to be 1.3 ± 0.21 nm (Fig. 2f). Notably, the mean diameter of our Mo_2C and MoN clusters (< 2 nm) ranks among the smallest metal clusters that have been reported so far for various electrocatalysis (Table S1 in Supporting information). Small clusters also play an important role in electrocatalytic reactions [27]. Moreover, Wang and co-workers [28] found that single Mo atoms (Mo-NC_2) and Mo_2C nanoparticle both have good performance in NRR by theoretical calculations and experiments.

X-ray photoelectron spectroscopy (XPS) was employed to analyze the element composition and corresponding chemical state of the surface in Fig. 3a, the presence of Mo, C, N and O elements was affirmed. The inductively coupled plasma atomic emissions spectrometry (ICP-AES) shows the actual loading of Mo is 1.08 wt%. No signal of Zn was detected, suggesting the Zn species have been removed from ZIF-8 by a heat treatment at high temperature, which is consistent with the results of XRD [29]. Fig. 3b shows high-resolution XPS spectra of Mo 3d with three pairs of peaks. Binding energies located at 235.6 eV (Mo $3d_{3/2}$) and 232.5 eV (Mo $3d_{5/2}$) were assigned to Mo^{6+} [30]. The characteristic Mo $3d_{3/2}$ and Mo $3d_{5/2}$ peaks of Mo^{4+} appeared at 232.3 and 229.2 eV, respectively. The above high valences of Mo (Mo^{4+} and Mo^{6+}) resulted from the surface oxidation of Mo (MoO_2 and MoO_3/MoO_x), which should be due to their gradual superficial oxidation when exposed to air [31,32]. Notably, another doublet at binding energies of 228.4 and 235.8 eV derived from Mo clusters were corresponding to $Mo^{\delta+}$, demonstrating the formation of Mo-N_xC species and Mo_2C/Mo_2N clusters, which was consistent with the results observed from HAADF-STEM images [33]. In Fig. 3c, four typical peaks at binding energies of around 398, 399, 401 and 403 eV were assigned to pyridinic-N, pyrrolic-N, graphitic-N and oxidized-N, respectively [34,35]. Besides, an accompanying minor Mo 3p was also observed. It is worth noticing that a relatively weak peak emerged at about 396 eV in N 1s spectrum verified the formation of Mo-N bonds, which suggested the existence of Mo-N_xC species and MoN clusters in the sample [36,37]. The binding

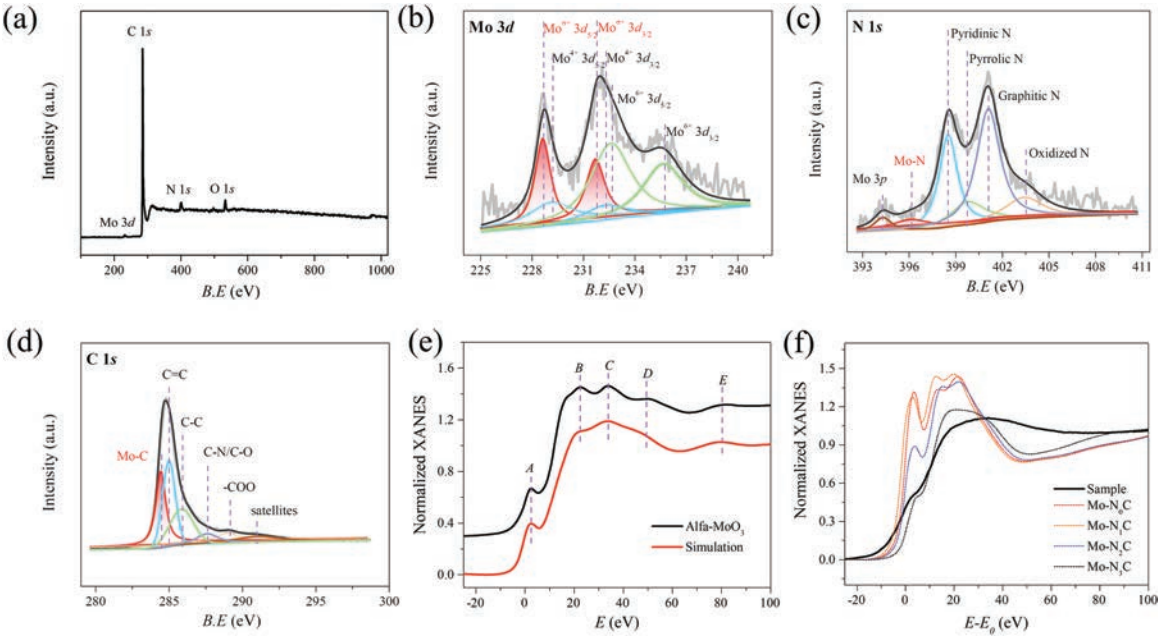

Fig. 3. (a) XPS survey spectra, (b) high-resolution Mo 3d, (c) N 1s and (d) C 1s XPS spectra of Mo-SA/Mo_2C-MoN-Cs, (e) Comparison between the XANES experimental spectra of α-MoO_3 at Mo K edge (solid black line) and the theoretical spectra calculated with the depicted structures (solid red line). (f) The normalized XANES at the Mo K-edge of different samples including the sample of Mo-SA/Mo_2C-MoN-Cs.

situation of carbon can be divided into five peaks. The presence of Mo—C bonds (284.3 eV, Fig. 3d) demonstrated that the existence of Mo-N_xC species and Mo_2C clusters, corresponding to the HAADF-STEM images result. The peaks centered at 284.9 (C=C), 285.8 (C—C) and 287.6 eV (C—N/C—O) resulted from N-doped porous carbon, while the peak at 289.1 eV (—COO) was attributed to the surface oxidized carbon or adsorbed oxygen-containing species [38].

Having this monodisperse Mo-SA/Mo_2C-MoN-Cs catalyst in hand, we are able to identify the structure related to Mo atoms. It has been well established that X-ray absorption near-edge structure (XANES) spectroscopy is a powerful technique to determine the chemical state and coordination environment of the center atoms in the sample [39–42]. First, finite difference methods for near-edge structure is used to calculate the α-MoO_3 standard sample (ICSD: #158255) to determine the relevant parameters used in the calculation of Mo K-edge XANES spectra of the as-prepared sample (Fig. 3e). Fig. 3f shows the XANES at the Mo K-edge of the Mo-SA/Mo_2C-MoN-Cs as well as of several reference samples, such as Mo-N_0C, Mo-N_1C, Mo-N_2C, Mo-N_3C. Based on the fitting parameters on the α-MoO_3 standard sample, the XANES of each theoretical calculation optimized model is simulated. From the change trend, it can be seen that Mo-N_3C is relatively close to the experimental spectra. Meanwhile, the trend of Mo-N_3C is not coinciding to the experimental date exactly, it may be because of the existence of Mo_2C/MoN clusters.

The theoretical study predicted that single Mo atoms immobilized on defective boron nitride monolayers can be a potential NRR electrocatalyst [43]. However, the further understanding of single Mo atoms supported on N-doped carbon for NRR system is deficient. Based on the HAADF, XANES and XPS characterization results, the binding energy of carbon-based materials with Mo atoms at different N-doping concentrations was studied by DFT calculations, as shown in Table S2 (Supporting information). We simulated the influence of different N concentrations by changing the number of N atoms that bonded with Mo (Fig. 4a and Fig. S1 in Supporting information). Under different number of N-coordination in the chemical structure of the Mo-N_xC moieties, the binding

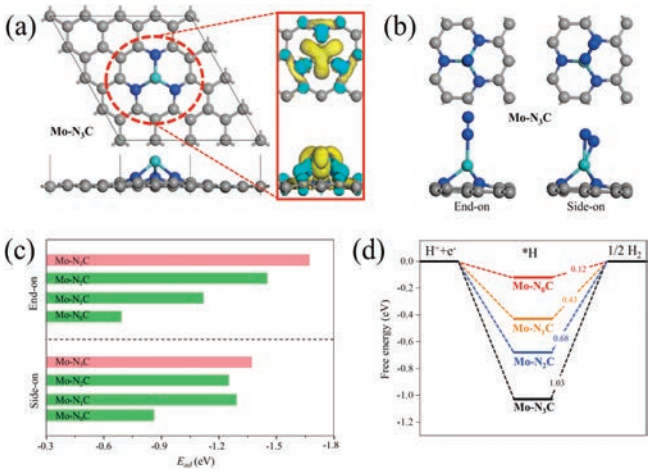

Fig. 4. (a) Top and side views of the Mo-N_3C moiety. Hereafter, the blue, gray, and cyan spheres represent N, C and Mo, respectively. Inset: The charge density difference (CDD) of the Mo-N_3C moiety cyan and yellow represent charge depletion and accumulation, respectively. The isosurface value of CDD is 0.03 e/Å^3. (b) Top and side views of the two most stable adsorption configurations of N_2 on the Mo-N_3C moiety. (c) The adsorption energy (E_{ad}) of N_2 molecules are adsorbed on Mo-doped graphene with different N contents (Including the end-on and side-on adsorption configurations of N_2 molecules and (d) the free energy diagrams of HER on the Mo-N_xC moieties with different N atom numbers.

energy of Mo atoms embedded in carbon-based materials was less than −4 eV, indicating that Mo atoms can be stably embedded in corresponding carbon-based materials. At the same time, the study found that as the number of N-coordination in the Mo-N_xC moieties increases, the positive charge of Mo atoms increases. In order to gain a deeper insight into the electronic properties of Mo-N_XC, we calculated the highest occupied molecular orbitals (HOMO) and the lowest unoccupied molecular orbitals (LUMO) for it (Fig. S2 in Supporting information). The results show that both HOMO and LUMO of Mo-N_xC are mainly distributed on Mo atoms. The molecular orbital that acts first in the chemical reaction

is the frontier molecular orbital. Among them, HOMO is easy to lose electrons and acts as electron donors, while LUMO has a strong affinity for electrons and acts as electron acceptors. Therefore, Mo atoms are activated, which may serve as active sites for further catalytic reactions on Mo-N_xC [44,45].

We then calculated the adsorption of N_2 molecules on carbon-based materials at different N-doping concentrations. The end-on and side-on configurations of N_2 adsorption were considered. In the four models studied, Mo atoms are used as active sites to effectively chemisorb N_2 molecules (Fig. 4b, Fig. S3 and Table S3 in Supporting information). The structure and charge analysis reveal that as the number of N-coordination in the Mo-N_xC moieties increases, the adsorption energy of N_2 decreases. It suggests the Mo-N_3C moiety has the best performance of N_2 adsorption (Fig. 4c). Besides, both the N—N bond length and the negative charge of the N_2 molecules increase. The stretching of the N—N bond and the massive transfer of electrons from the Mo-N_xC moieties to the N_2 molecules indicate that the N_2 molecules are effectively activated. As the number of N-coordination in the Mo-N_xC moieties increases, the ability to activate N_2 molecules increases, promoting the further reduction process. As known, HER is the main competitive reaction of NRR [46–48]. We then use DFT to calculate the changes in HER free energy on the four models. For HER, carbon-based materials without N-doping are more conducive to hydrogen production, and the rate-limiting potential is only 0.12 V (Fig. 4d). As the number of N-coordination in the chemical structure of the Mo-N_xC moieties increases, the rate-limiting potential of the HER increases, indicating that the model can effectively inhibit HER.

In summary, isolated Mo single atoms combined with some ultrasmall Mo_2C/MoN clusters were synthesized. The catalyst mainly exited in the form of Mo single atoms (Mo-N_3C). The mean diameter (< 2 nm) of Mo_2C/MoN clusters ranks among the smallest size reported. DFT calculations indicate that single Mo atoms in Mo-N_3C structure as the active sites have the best N_2 adsorption capability with the most charge transfer from Mo-N_3C to N_2, which is beneficial for the further reduction process. Further experimental work is underway. This work provides a meaningful reference to SACs related NRR in terms of experiments.

Declaration of competing interest

The authors report no declarations of interest.

Acknowledgments

Y. Lei thanks the financial support from the Hunan Provincial Science and Technology Plan Project (Nos. 2017TP1001, 2020JJ4710). C. He thanks the National Natural Science Foundation of China (No. 21603109), the Henan Joint Fund of the National Natural Science Foundation of China (No. U1404216). L. Chen thanks the postdoctoral research funding plan in Central South University (No. 140050022). W. Liu thanks the Fundamental Research Funds for the Central Universities (No. DUT20RC(3)021). We thank the 1W1B station for XAFS measurements in Beijing Synchrotron Radiation Facility (BSRF).

Appendix A. Supplementary data

Supplementary material related to this article can be found, in the online version, at doi:https://doi.org/10.1016/j.cclet.2020.11.013.

References

[1] C. Zhao, X. Dai, T. Yao, et al., J. Am. Chem. Soc. 139 (2017) 8078–8081.
[2] J. Liu, ACS Catal. 7 (2017) 34–59.
[3] L. Han, L.J. Zhang, H. Wu, et al., Adv. Sci. 6 (2019) 1900006.
[4] Y. Cheng, S. He, S.F. Lu, et al., Adv. Sci. 6 (2019) 1802066.
[5] X. Li, H. Rong, J. Zhang, D. Wang, Y. Li, Nano Res. 13 (2020) 1842–1855.
[6] J. Yang, W. Li, D. Wang, Y. Li, Small Struct. (2020), doi:http://dx.doi.org/10.1002/sstr.202000051.
[7] J. Zhang, C. Zheng, M. Zhang, et al., Nano Res. 13 (2020) 3082–3087.
[8] W. Peng, M. Luo, X. Xu, et al., Adv. Energy Mater. 10 (2020) 2001364.
[9] J.J. Guo, T. Tadesse Tsega, I. Ul Islam, et al., Chin. Chem. Lett. 31 (2020) 2487–2490.
[10] Y. Hang, W. Qiang, L. Wei, S.P. Cheng, Chin. Chem. Lett. 31 (2020) 1768–1772.
[11] J. Sun, W.H. Kong, Z.Y. Jin, et al., Chin. Chem. Lett. 31 (2020) 953–960.
[12] W. Xiong, X. Cheng, T. Wang, et al., Nano Res. 13 (2020) 1008–1012.
[13] T. Wu, H. Zhao, X. Zhu, et al., Adv. Mater. 32 (2020) 2000299.
[14] X. Lv, F. Wang, J. Du, et al., Sustain. Energy Fuels 4 (2020) 4469–4472.
[15] S. Zhang, M. Jin, T. Shi, et al., Angew. Chem. Int. Ed. 59 (2020) 13423–13429.
[16] Y. Chen, R. Guo, X. Peng, et al., ACS Nano 14 (2020) 6938–6946.
[17] F. Lü, S. Zhao, R. Guo, et al., Nano Energy 61 (2019) 420–427.
[18] C. Tang, Y. Jiao, B. Shi, et al., Angew. Chem. Int. Ed. 59 (2020) 9171–9176.
[19] Y.P. Lei, Y.C. Wang, Y. Liu, et al., Angew. Chem. Int. Ed. 59 (2020) 20794–20812.
[20] W. Chen, J. Pei, C.T. He, et al., Angew. Chem. Int. Ed. 56 (2017) 16086–16090.
[21] L. Han, X. Liu, J. Chen, et al., Angew. Chem. Int. Ed. 58 (2019) 2321–2325.
[22] G. Gao, Q. Xi, Y. Zhang, et al., Nanoscale 11 (2019) 1169–1176.
[23] P. Zhang, F. Sun, Z. Xiang, et al., Energy Environ. Sci. 7 (2014) 442–450.
[24] P. Yin, T. Yao, Y. Wu, et al., Angew. Chem. Int. Ed. 55 (2016) 10800–10805.
[25] X.F. Lu, L. Yu, J. Zhang, X.W. Lou, Adv. Mater. 31 (2019) 1900699.
[26] Y. Liu, C.Y. Song, Y.C. Wang, et al., Chem. Eng. J. 401 (2020) 126038.
[27] Y. Lei, F. Yang, H. Xie, et al., J. Mater. Chem. A 8 (2020) 20629–20636.
[28] Y. Ma, T. Yang, H. Zou, et al., Adv. Mater. 32 (2020) 2002177.
[29] Y. Wang, J. Wang, D. Wei, M. Li, ACS Appl. Mater. Interfaces 11 (2019) 35755–35763.
[30] J. Yang, F. Zhang, X. Wang, et al., Angew. Chem. Int. Ed. 55 (2016) 12854–12858.
[31] M. Xiang, D. Li, W. Li, B. Zhong, Y. Sun, Catal. Commun. 8 (2007) 513–518.
[32] J. Jiang, Q. Liu, C. Zeng, L. Ai, J. Mater. Chem. A 5 (2017) 16929–16935.
[33] Y. Wang, Z. Shi, Q. Mo, et al., ChemElectroChem 4 (2017) 2169–2177.
[34] Q.C. Wang, Y.J. Ji, Y. Lei, et al., ACS Energy Lett. 3 (2018) 1183–1191.
[35] Q.C. Wang, K. Ye, L. Xu, et al., Chem. Commun. 55 (2019) 14801–14804.
[36] S. Li, C. Cheng, A. Sagaltchik, et al., Adv. Funct. Mater. 29 (2019) 1807419.
[37] L. Zeng, S. Chen, J. van der Zalm, X. Li, A. Chen, Chem. Commun. 55 (2019) 7386–7389.
[38] L. Zhang, Z. Su, F. Jiang, et al., Nanoscale 6 (2014) 6590–6602.
[39] A.M. Gänzler, M. Casapu, A. Boubnov, et al., J. Catal. 328 (2015) 216–224.
[40] Q. Liu, Q. Wang, J. Wang, et al., Adv. Funct. Mater. (2020) 2000593.
[41] Q.C. Wang, Y. Lei, Y.C. Wang, et al., Energy Environ. Sci. 13 (2020) 1593–1616.
[42] Y.C. Wang, Y. Liu, W. Liu, et al., Energy Environ. Sci. 13 (2020) 4609–4624.
[43] J. Zhao, Z. Chen, J. Am. Chem. Soc. 139 (2017) 12480–12487.
[44] C. Yao, R. Wang, Z. Wang, et al., J. Mater. Chem. A 7 (2019) 27547–27559.
[45] C. He, R. Wang, H. Yang, S. Li, L. Fu, Appl. Surf. Sci. 507 (2020) 145076.
[46] Y. Sun, Z.Z. Deng, X.M. Song, et al., Nano Micro Lett. 12 (2020) 133.
[47] Q.C. Wang, Y. Lei, D.S. Wang, Y.D. Li, Energy Environ. Sci. 12 (2019) 1730–1750.
[48] Y.C. Wang, B. Liu, Y. Liu, et al., Chem. Commun. 56 (2020) 14019–14022.